Available online at www.sciencedirect.com
ScienceDirect
Journal of the European Ceramic Society 29 (2009) 621–628
www.elsevier.com/locate/jeurceramsoc

Improvement in sinterability and phase stability of hydroxyapatite and partially stabilized zirconia composites

Zafer Evis [a,*], Metin Usta [b], Isil Kutbay [b]

[a] *Department of Engineering Sciences, Middle East Technical University, Ankara 06531, Turkey*
[b] *Department of Materials Science and Engineering, Gebze Institute of Technology, Gebze, Kocaeli 41400, Turkey*

Received 5 November 2007; received in revised form 19 June 2008; accepted 4 July 2008
Available online 28 August 2008

Abstract

Composites of hydroxyapatite with partially stabilized zirconia with MgO or MgF_2 were pressureless sintered between 1000 °C and 1300 °C. The reactions and transformations of phases were verified by X-ray diffraction. For the hydroxyapatite and zirconia composites with MgO, calcium from the hydroxyapatite diffused into the zirconia phase, and the hydroxyapatite decomposed to tri-calcium phosphate at sintering temperatures higher than 1000 °C. Above about 1200 °C, $CaZrO_3$ was formed. Composites containing the MgF_2 decomposed slower than the composites with MgO, which was verified by the changes in the lattice volume of the hydroxyapatite left in these composites. Fluorine ions in MgF_2 diffused into hydroxyapatite, which resulted in thermal stability at high sintering temperatures. Composites with MgF_2 had higher hardness than those with MgO. The lowest porosity was found in a composite initially containing 10 wt% partially stabilized zirconia and 5 wt% MgF_2.

Keywords: Apatite; Sintering; MgF_2; Biomedical applications

1. Introduction

Hydroxyapatite (HA, $Ca_{10}(PO_4)_6(OH)_2$) has been widely used as a bulk implant material in non-load bearing areas of the body and as coatings on implant metals. Although HA has excellent biocompatibility properties, it is limited in use due to its brittle nature.[1,2] Composites of HA and zirconia can combine the biocompatibility of HA and the high strength of zirconia to be used in orthopedic applications.

To make HA–zirconia composites, calcium phosphate source chemicals and zirconia powders are mixed, cold pressed and then sintered at high temperatures.[3–7] Sintering temperature is important in determining the final properties of the composite. Moreover, sintering conditions such as microwave sintering, spark plasma spraying, hot pressing, and hot isosotatic pressing could also be used in addition to pressureless air sintering.[8–12] For example, although pure HA starts to decompose to tri-calcium phosphate (TCP) at ∼1300 °C, a second phase forms well below 1300 °C in the presence of ZrO_2.[3,4,7,13] Kim et al.[4] enhanced the sinterability of 3 mol% Y_2O_3–ZrO_2 (up to 40 vol.%)–HA composites by increasing the green density of the composites through cold isostatic pressing and the addition of small amounts of CaF_2. In these composites, they observed the decomposition of HA first into β-TCP at a temperature of 1350 °C, and then at temperatures above 1350 °C, β-TCP became unstable and transformed to α-TCP. Thus, the presence of zirconia has a great influence on phase changes in HA at temperatures different than that observed with pure HA. Moreover, improved osteoblast adhesion was measured on HA–partially stabilized zirconia composites sintered at 900 °C and with 10 wt% partially stabilized and 90 wt% HA composite.[14]

Yttria-stabilized zirconia and hydroxyapatite composites were developed to be durable and bioactive.[8,15] When the zirconia was added into HA, the grain sizes of HA became smaller.[16] For example, HA and zirconia composites with grain sizes smaller than 100 nm had improved bending strength.[16]

HA–ceramic composites, especially HA–zirconia composites, have shown promising improvements in strength, hardness and toughness as compared to HA itself.[17,18] On the other hand, decomposition of HA, which forms second phases, and phase transformation of partially stabilized zirconia from tetragonal to cubic structure can diminish the mechanical properties of these

* Corresponding author. Tel.: +90 312 2104450; fax: +90 312 2104462.
E-mail address: evis@metu.edu.tr (Z. Evis).

0955-2219/$ – see front matter © 2008 Elsevier Ltd. All rights reserved.
doi:10.1016/j.jeurceramsoc.2008.07.020

composites.[17,19] There is an agreement that the addition of zirconia to the HA causes it to decompose at lower temperatures in pressureless sintering, so that several workers have used hot pressing to reach higher density.[20–22] At sintering temperatures higher than 1000 °C, calcium from the HA diffused into the zirconia phase, and the HA decomposed to TCP.[23] Above about 1200 °C, $CaZrO_3$ was formed.[23] Moreover, when the Mg partially stabilized zirconia and HA composites were sintered in air at 1250 °C for 4 h, HA decomposed into β-TCP and $CaZrO_3$.[24]

Despite the fact that several studies have characterized the partially stabilized zirconia and HA composites, no work has been conducted to determine and compare the effect of MgO and MgF_2 on the phase transformations in HA and partially stabilized zirconia composites. In the present work, HA and partially stabilized zirconia composites with MgO or MgF_2 were prepared by air sintering at 1000 °C, 1100 °C, 1200 °C, and 1300 °C for 1 h and the resultant composites were characterized with microhardness, density, X-ray diffraction (XRD), and scanning electron microscopy (SEM).

2. Materials and methods

2.1. Bioceramics materials and synthesis

The materials used in this research were composites of HA with partially stabilized zirconia with the addition of MgO or MgF_2. The abbreviations, description and the composition of the samples of interest to the present study are shown in Table 1.

HA was synthesized by mixing reagent grades of calcium nitrate and reagent grade di-ammonium hydrogen phosphate solutions in the alkaline pH region.[25,26] The powders of the PSZ (3% Y_2O_3–97% ZrO_2) (Zirconia Sales Inc.) were then mixed with HA and reagent grade of MgO (or MgF_2) powders. To accomplish this, the dried HA particles were ground to 75 μm size (−200 mesh) powders using an agate mortar and pestle.

Table 1
Abbreviations and compositions of the samples

Name	Abbreviation	Composition
Hydroxyapatite	HA	–
Tri-calcium phosphate	TCP	–
Partially stabilized zirconia	PSZ	3 mol% Y_2O_3-doped ZrO_2
Monoclinic zirconia	m-ZrO_2	–
Tetragonal zirconia	t-ZrO_2	–
Cubic zirconia	c-ZrO_2	–
Hydroxyapatite and partially stabilized zirconia composites	10ZHAO	10 wt% PSZ + 85 wt% HA + 5 wt% MgO
	25ZHAO	25 wt% PSZ + 70 wt% HA + 5 wt% MgO
	40ZHAO	40 wt% PSZ + 55 wt% HA + 5 wt% MgO
	10ZHAF	10 wt% PSZ + 85 wt% HA + 5 wt% MgF_2
	25ZHAF	25 wt% PSZ + 70 wt% HA + 5 wt% MgF_2
	40ZHAF	40 wt% PSZ + 55 wt% HA + 5 wt% MgF_2

They were then calcined at 900 °C for 1 h and mixed with PSZ powders by ball milling. Mixed powders were sintered in air at 1000 °C, 1100 °C, 1200 °C, and 1300 °C for 1 h in a high temperature box furnace. They were heated and cooled in the furnace.

2.2. Characterization methods

Sample surfaces were examined by a Philips XL30 SFEG scanning electron microscope (SEM) at 7–10 kV to determine the grain size of the composites. Samples were gold coated with a Polaron-SC7610 Sputter in vacuum before examination in the SEM. Grain size was determined by the intercept method. A 20-cm circumference circle was used to determine grain sizes of the samples. The following formula was used to determine the grain sizes from the SEM micrographs.[27]

$$G_{\text{ave}} = \frac{L}{NM} \tag{1}$$

where G_{ave} is the average grain size, L the circumference of the circle (20 cm), N the number of intersections along 20 cm circumference line and M is the magnification.

The bulk density of the sintered samples was determined by measuring the weight and volume of the sintered composites. The theoretical density of the composites (components a and b) was calculated from the known weights, W and densities, ρ by the following formula:

$$\text{density } (\text{g/cm}^3) = \frac{W_a + W_b}{(W_a/\rho_a) + (W_b/\rho_b)} \tag{2}$$

where component "a" is PSZ and component "b" is HA and/or TCP. Density of HA and TCP was assumed to be the same for the simplicity of composite density calculation.

Samples were cut perpendicular to their cross-sections using a diamond saw and polished for the micro-hardness measurements. After samples were mounted into a 20-mm diameter epoxy, they were polished from 75 μm surface roughness to below 100 nm surface roughness. The micro-hardness of the samples were measured by an Instron Wolpert Microhardness tester 2100 series equipped with a Vickers diamond indenter with a load of 500 g. For each sample, 20 measurements were performed.

All the samples were pulverized using an agate mortar and pestle before the XRD characterization of them. After the pulverizing, they were pressed onto a dimpled quartz glass. Then, they were characterized by a Rigaku Dmax 2200 XRD diffractometer with Cu Kα radiation at 40 kV/40 mA at lambda = 1.54178 Å. Each sample was scanned from 5° to 70° in 2θ with a step size of 0.02° and scanning rate of 1° min^{-1}. The hexagonal lattice parameters of HA were calculated by successive approximations according to standard procedures.[28] The volume of the each unit cell was calculated by the following formula $V = 2.589a^2c$. To determine the phases present, XRD peak positions were compared with the International Centre for Diffraction Data (ICDD) files.

To determine the decomposition of HA into TCP, the relative amounts of phases were determined from the most intense

XRD peaks of the HA and α-/β-TCP.[28,29] It is assumed that the concentrations (wt%) of HA and TCP phases are proportional to their peak heights in the mixtures. First the ratio R_O of the peak heights of HA to that of α- or β-TCP was determined for mixtures of known concentrations of HA and α- or β-TCP. Lower limit of detection was about 1 wt% of the known mixture of HA and TCP. It was found that the ratio R_O did not depend on the relative amounts of HA and TCP; the values of R_O found were 1.755 for $R_O = I_H/I_\beta$ and $R_O = I_H/I_\alpha = 2.217$, where I_H, I_β and I_α are the XRD peak heights for HA, β- and α-TCP, respectively in mixtures of known concentrations. Then for mixtures of HA and β-TCP:

$$\frac{W_H}{W_\beta} = \frac{R}{R_O} \quad (3)$$

where W_H and W_β are the weight fractions of HA and β-TCP, respectively. A similar formula for mixtures of HA and α-TCP, with W_α substituted for W_β, was used.

3. Results

The average grain sizes of 10ZHAO and 10ZHAF composited sintered at 1100 °C determined from the SEM micrographs is presented in Fig. 1. In addition to images in Fig. 1, grain size changes of the composites with respect to sintering temperature between 1000 °C and 1300 °C are seen in Fig. 2. Specifically, for 10ZHAF, the grain size increased from 226 nm to 942 nm when sintering was increased from 1000 °C to 1300 °C. In particular, there was more grain growth in the composites after sintering between 1200 °C and 1300 °C. Similar results were seen for the other HA and PSZ composites. 10ZHAF samples had smaller grain sizes than the 10ZHAO samples (Figs. 1 and 2) at all of the sintering temperatures.

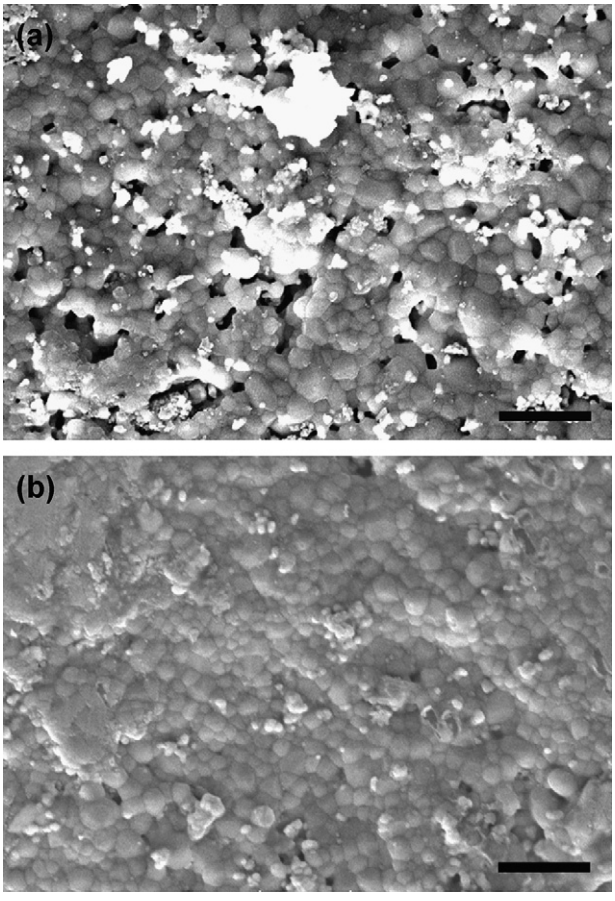

Fig. 1. SEM images of 10ZHAO (a) and 10ZHAF (b) composites sintered at 1100 °C. Scale bars = 2 μm.

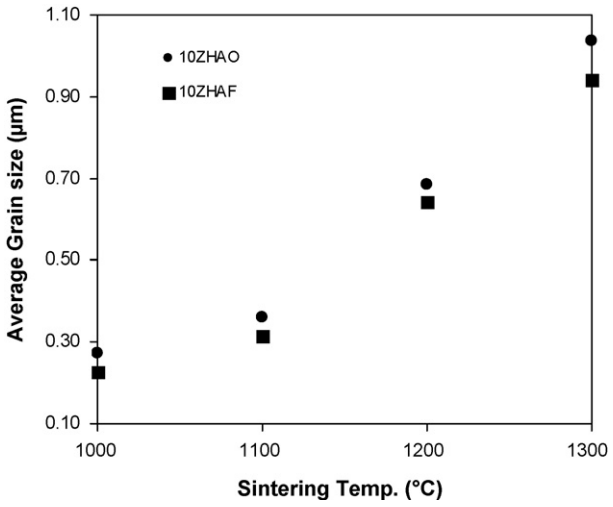

Fig. 2. Average grain sizes of the 10ZHAO and 10ZHAF composites sintered between 1000 °C and 1300 °C for 1 h.

The relative densities of the composites are shown in Figs. 3 and 4. Increasing the sintering temperature from 1000 °C to 1300 °C and reducing the zirconia content from 40 wt% to

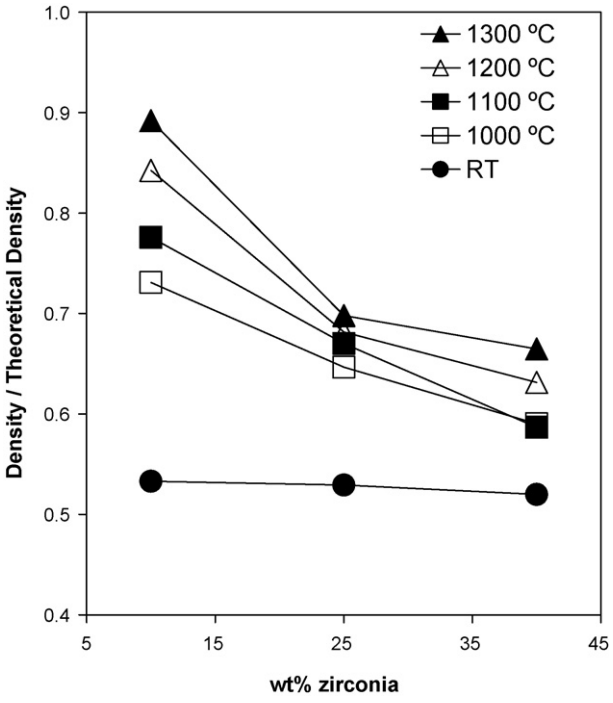

Fig. 3. Density/theoretical density as a function of the amount of partially stabilized zirconia in the composites with 5 wt% MgO sintered at 1000 °C, 1100 °C, 1200 °C, and 1300 °C for 1 h. Theoretical density was calculated by Eq. (1).

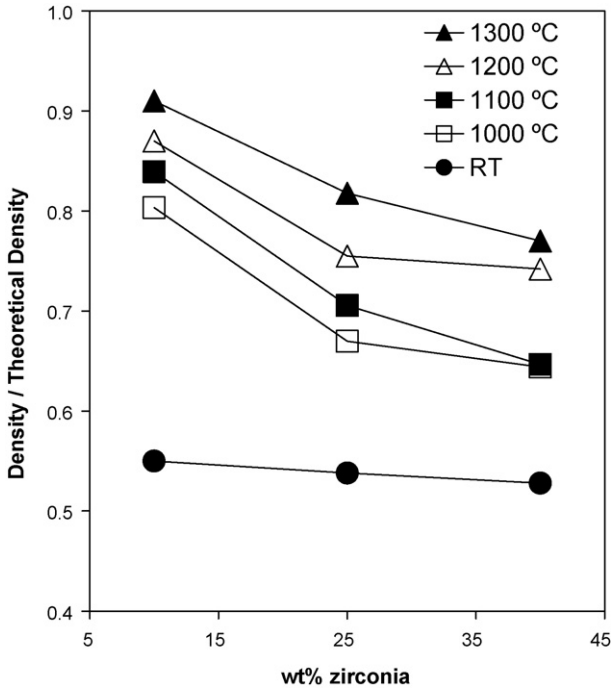

Fig. 4. Density/theoretical density as a function of the amount of partially stabilized zirconia in the composites with 5 wt% MgF_2 sintered at 1000 °C, 1100 °C, 1200 °C, and 1300 °C for 1 h. Theoretical density was calculated by Eq. (1).

10 wt% in the composites improved the density. The composites containing 5 wt% MgF_2 (Fig. 4) had better densification than the composites with 5 wt% MgO (Fig. 3). The maximum relative density (91%) was found for the composite 10ZHAF sintered at 1300 °C for 1 h.

Hardness measurements for 10ZHAO and 10ZHAF showed that 10ZHAF had higher hardness values than 10ZHAO for all of the sintering temperatures (Fig. 5).

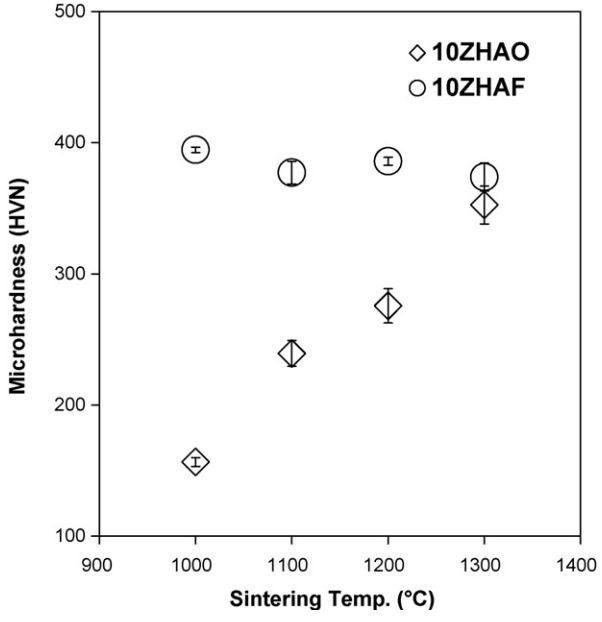

Fig. 5. Microhardness results of 10ZHAO and 10ZHAF composites.

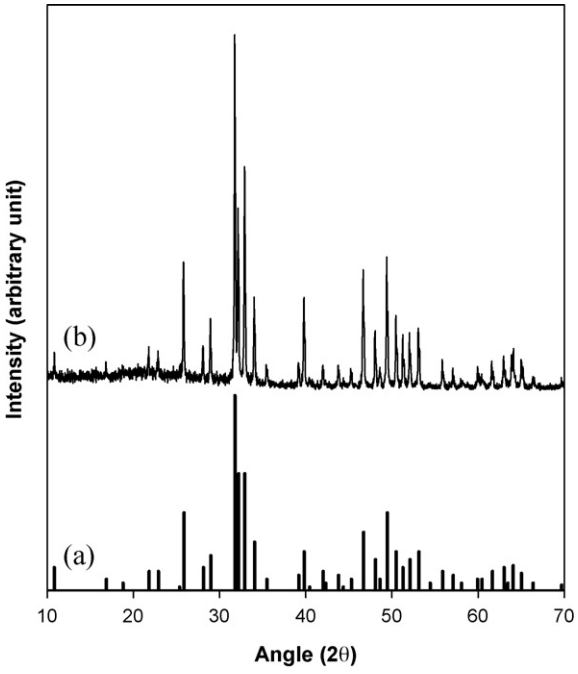

Fig. 6. X-ray diffraction patterns of (a) pure HA (ICDD #9–432) and (b) synthetic HA sintered in air at 1100 °C for 1 h. All peaks correspond to HA.

When the synthetic HA made by precipitation method was sintered at 1100 °C for 1 h, all the XRD peaks were corresponding to pure HA as seen in Fig. 6. XRD patterns of 10ZHAO, 25ZHAO, and 40ZHAO composites sintered at 1000 °C, 1100 °C, 1200 °C and 1300 °C for 1 h are presented in Figs. 7–9. As the sintering temperature increased, the PSZ began to transform to c-ZrO_2. HA started to decompose to a mixture of α- and β-TCP at 1000 °C; at 1300 °C this decomposition was nearly complete, and the TCP was entirely α phase. When the amount of the zirconia increased in the composites, HA decomposed faster at higher sintering temperatures. Moreover, HA was decomposed much faster in the composites with MgO. This was verified by the changes in the hexagonal lattice parameters of HA left in the composites (Table 2). Hexagonal lattice volumes of HA left in 10ZHAO were greater than that of pure HA (Table 2). This showed that HA in 10ZHAO was Ca^{2+}

Table 2
Hexagonal lattice parameters of HA present in the 10ZHAO and 10ZHAF composites after the sintering between 1000 °C and 1300 °C

Sample ID	Sintering temp. (°C)	Lattice parameters (Å)		Volume (Å^3)	Avol. (Å^3)
		a	c		
HA	1100	9.4264	6.8884	1584.7	
10ZHAO	1000	9.4402	6.8957	1591.0	6.3
	1100	9.4418	6.9018	1593.0	8.3
	1200	9.4215	6.8877	1582.9	−1.8
	1300	9.4231	6.8967	1585.5	0.8
10ZHAF	1000	9.3814	6.8884	1569.6	−15.1
	1100	9.394	6.8908	1574.4	−10.3
	1200	9.3765	6.8848	1567.1	−17.6
	1300	9.3553	6.8679	1556.2	−28.5

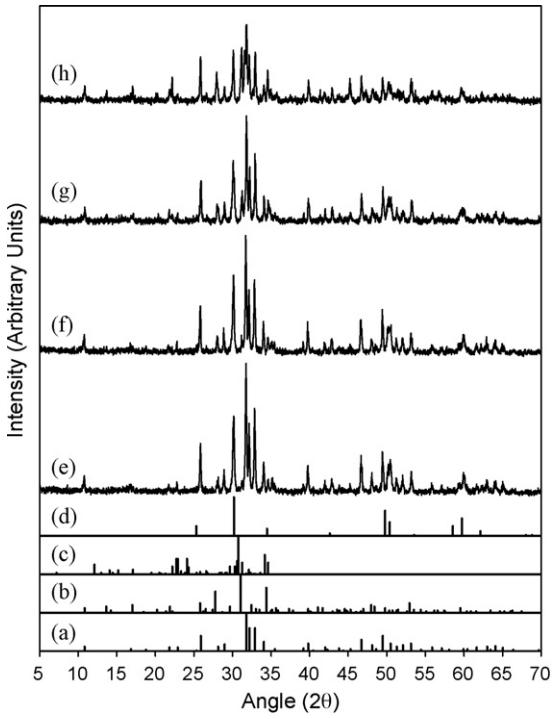

Fig. 7. X-ray diffraction spectra of the air sintered composites: (a) HA (ICDD #9–432); (b) β-TCP (ICDD #9–169); (c) α-TCP (ICDD #9–348); (d) t-ZrO_2 (ICDD #17–923); (e) 10ZHAO, 1000 °C, 1 h; (f) 10ZHAO, 1100 °C, 1 h; (g) 10ZHAO, 1200 °C, 1 h; (h) 10ZHAO, 1300 °C, 1 h.

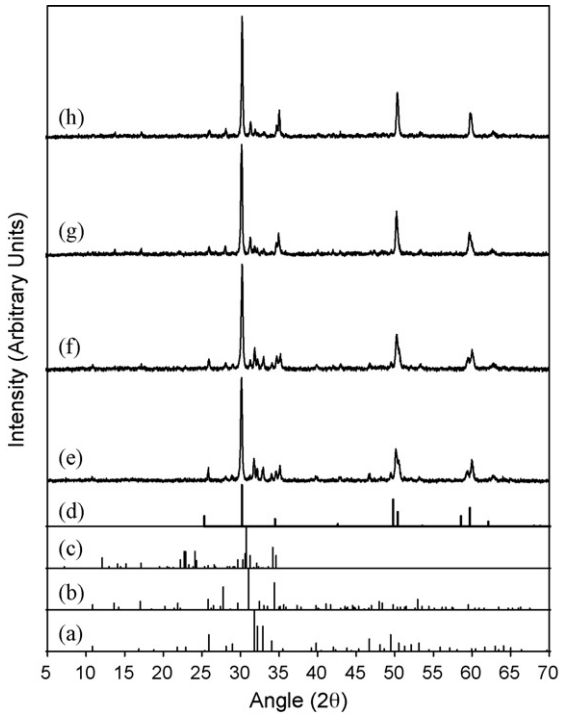

Fig. 9. X-ray diffraction spectra of the air sintered composites: (a) HA (ICDD #9–432); (b) β-TCP (ICDD #9–169); (c) α-TCP (ICDD #9–348); (d) t-ZrO_2 (ICDD #17–923); (e) 40ZHAO, 1000 °C, 1 h; (f) 40ZHAO, 1100 °C, 1 h; (g) 40ZHAO, 1200 °C, 1 h; (h) 40ZHAO, 1300 °C, 1 h.

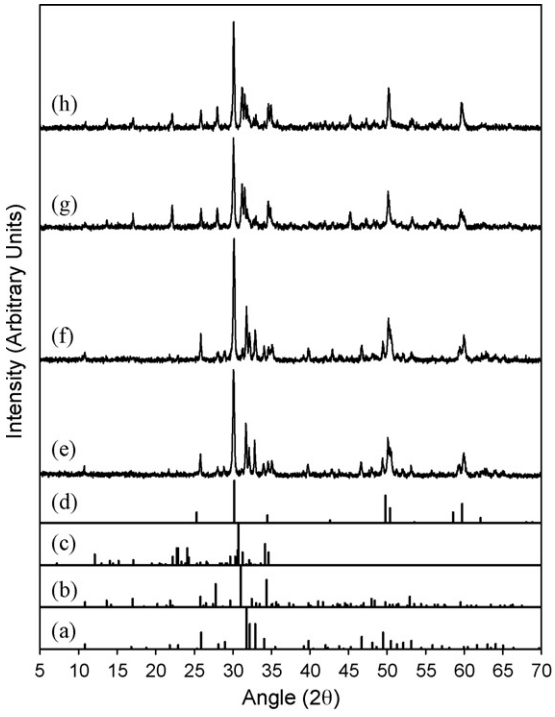

Fig. 8. X-ray diffraction spectra of the air sintered composites: (a) HA (ICDD #9–432); (b) β-TCP (ICDD #9–169); (c) α-TCP (ICDD #9–348); (d) t-ZrO_2 (ICDD #17–923); (e) 25ZHAO, 1000 °C, 1 h; (f) 25ZHAO, 1100 °C, 1 h; (g) 25ZHAO, 1200 °C, 1 h; (h) 25ZHAO, 1300 °C, 1 h.

and OH^- deficient. HA in 10ZHAO slightly started to decompose to second phases at 1000 °C. Moreover, HA in 25ZHAO and 40ZHAO started to transform to β-TCP at 1000 °C. Percentage of HA transformed into second phases (e.g. TCP, calcium zirconate) in the composites containing 5 wt% MgO is shown in Table 3. Transformation of HA into TCP was calculated by Eq. (3). When wt% of zirconia and sintering temperature were increased, more HA decomposed into second phases.

XRD patterns of 10ZHAF, 25ZHAF, and 40ZHAF composites sintered at 1000 °C, 1100 °C, 1200 °C, and 1300 °C for 1 h are presented in Figs. 10–12. Tetragonal zirconia in these composites was stable after the sintering at 1000 °C and 1100 °C. Moreover, this t-ZrO_2 was converted to c-ZrO_2 after the sintering at 1200 °C and 1300 °C. HA in all of the composites containing 5 wt% MgF_2 was stable after all the sinterings between 1000 °C and 1300 °C. This was verified by the change in the hexagonal lattice parameters of HA left in the composites (Table 2). Hexagonal lattice volumes of HA left in 10ZHAF were smaller than

Table 3
%HA decomposed to TCP in the HA–zirconia composites containing 5 wt% MgO

Sample ID	Sintering temp. (°C)			
	1000	1100	1200	1300
10ZHAO	12	19	31	52
25ZHAO	15	27	61	78
40ZHAO	25	46	77	83

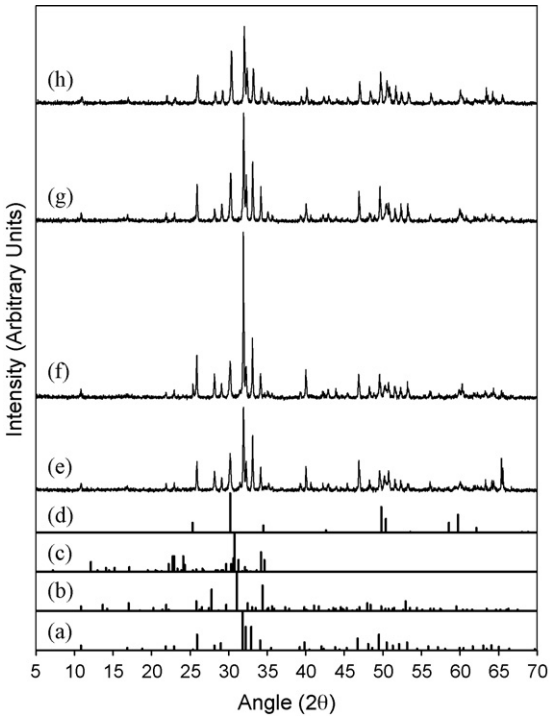

Fig. 10. X-ray diffraction spectra of the air sintered composites: (a) HA (ICDD #9–432); (b) β-TCP (ICDD #9–169); (c) α-TCP (ICDD #9–348); (d) t-ZrO_2 (ICDD #17–923); (e) 10ZHAF, 1000 °C, 1 h; (f) 10ZHAF, 1100 °C, 1 h; (g) 10ZHAF, 1200 °C, 1 h; (h) 10ZHAF, 1300 °C, 1 h.

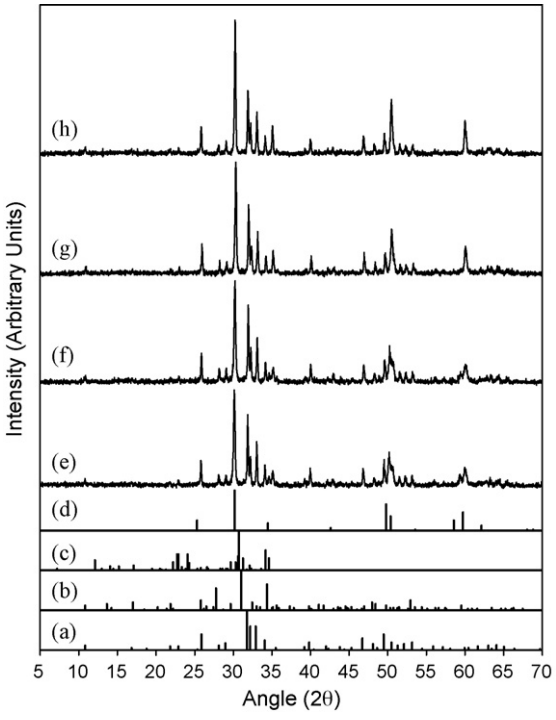

Fig. 11. X-ray diffraction spectra of the air sintered composites: (a) HA (ICDD #9–432); (b) β-TCP (ICDD #9–169); (c) α-TCP (ICDD #9–348); (d) t-ZrO_2 (ICDD #17–923); (e) 25ZHAF, 1000 °C, 1 h; (f) 25ZHAF, 1100 °C, 1 h; (g) 25ZHAF, 1200 °C, 1 h; (h) 25ZHAF, 1300 °C, 1 h.

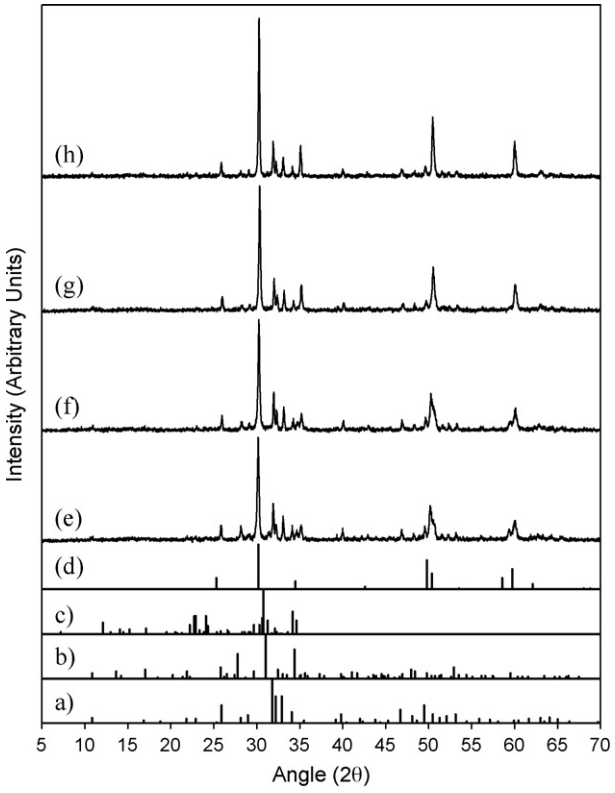

Fig. 12. X-ray diffraction spectra of the air sintered composites: (a) HA (ICDD #9–432); (b) β-TCP (ICDD #9–169); (c) α-TCP (ICDD #9–348); (d) t-ZrO_2 (ICDD #17–923); (e) 40ZHAF, 1000 °C, 1 h; (f) 40ZHAF, 1100 °C, 1 h; (g) 40ZHAF, 1200 °C, 1 h; (h) 40ZHAF, 1300 °C, 1 h.

that of pure HA (Table 2). This showed that HA in 10ZHAF was doped with F^-.

4. Discussion

The highest relative density (91%) was found after sintering the 10ZHAF composite at 1300 °C (Fig. 4). Sintering at lower temperatures or higher ZrO_2 with 5 wt% MgO contents caused higher porosity. This was due to the production of water during the sintering in the composites with MgO. This resulted in higher hardness values for 10ZHAF composites than that of 10ZHAO composites. In the HA and zirconia composites with MgO, HA decomposes faster into TCP, CaO and water.

The decrease in the decomposition of the HA by addition of 5 wt% MgF_2 to the sintering powders of HA and partially stabilized composites (10ZHAF, 25ZHAF, and 40ZHAF led to lower porosity in the sintered composites with MgF_2 than the composites with MgO because of the less water produced during sintering. This reduced porosity led to higher densification and more phase stability of the sintered composites with 5 wt% MgF_2.

When the starting zirconia powder contains 3 mol% Y_2O_3, it is in the tetragonal structure, with no m-ZrO_2 phase present (Figs. 7–12). This powder is more reactive with MgO after all of the sintering temperatures, leading to more decomposition of HA in the composites of 10ZHAO, 25ZHAO, and 40ZHAO. Perhaps the reason for this more reactivity is that the diffusion

of MgO into ZrO_2 and HA react with them to produce second phases. The decomposition reaction of HA into second phases is

$$Ca_{10}(PO_4)_6(OH)_2 \leftrightharpoons 3Ca_3(PO_4)_2 + CaO + H_2O \quad (4)$$

The CaO formed by the decomposition of HA (reaction (4)) can react with zirconia to form $CaZrO_3$:

$$CaO + ZrO_2 \leftrightharpoons CaZrO_3 \quad (5)$$

This reaction appears to take place only at 1200 °C or above, from Figs. 7–9. Moreover, MgO present in the HA–zirconia composite also reacts with t-ZrO_2 to transform it to c-ZrO_2:

$$MgO + \text{t-}ZrO_2 \leftrightharpoons \text{MgO-doped c-}ZrO_2 \quad (6)$$

HA begins to decompose by the reaction (4) at sintering temperatures above about 1150 °C in ambient atmosphere. Tetragonal-zirconia and MgO in the HA composites without added fluoride accelerates this decomposition of HA. One reason for this more reaction is that the CaO formed in reaction (4) can react with the t-ZrO_2 to form $CaZrO_3$ (reaction (5)).

Formation of $CaZrO_3$ in the sintered 10ZHAO, 25ZHAO, and 40ZHAO composites was confirmed by XRD. Removal of the CaO in reaction (5) than drives Eq. (4) to further decomposition of the HA. Moreover, MgO plays also an important role in this decomposition. It also accelerates this decomposition.

Another process that removes CaO from HA is dissolution of CaO into t-ZrO_2 as seen in reaction (7).

$$CaO + \text{t-}ZrO_2 \leftrightharpoons \text{c-}ZrO_2 \quad (7)$$

The original t-ZrO_2 (PSZ) transforms to the cubic phase as CaO dissolves in it; the tetragonal phase in PSZ has a distorted fluorite structure, in which oxides such as CaO, MgO, and Y_2O_3 show considerable solid solubility. X-ray results showed that some of the tetragonal-zirconia transformed to the cubic phase after sintering of the composites with MgO.

The addition of 5 wt% MgF_2 to the tetragonal-zirconia and HA mixtures (10ZHAF, 25ZHAF, and 40ZHAF) strongly reduced the tendency of the HA to decompose during sintering. We propose that this reduced tendency of the HA is because of partial substitution F^- ions for OH^- ions in the apatite structure.[30–34] This substitution of F^- ions for OH^- ions can be written as

$$Ca_{10}(PO_4)_6(OH)_2 + MgF_2 \rightarrow Ca_{10}(PO_4)_6F_2 + MgO + H_2O \quad (8)$$

This substitution (reaction (8)) takes place prior to sintering, even at temperatures below 1000 °C.[31] The water formed in reaction (8) devolatilizes the powder mixture. Devolatilization reactions in principle are equilibrium phenomena. However, as the volatile component (H_2O in reaction (8)) is allowed to escape, equilibrium can never be attained and as a result, only the right side of the reaction equation is favoured. As a result, this devolatilization promotes to completion of reaction (8) from left to the right, resulting in formation of fluorapatite ($Ca_{10}(PO_4)_6F_2$).[32]

The OH^- ions in the pure HA are positioned in openings parallel to the *c*-axis.[33–35] Ionic radius of OH^- ions is greater than that of the fluoride ions. Therefore, doping of F^- ions in HA for OH^- ions leads to a shrinkage of the unit cell volume of the HA.[30,33] Consistent with this shrinkage we found a decrease in the hexagonal lattice volume of HA in the composites with 5 wt% MgF_2 addition, as seen in Table 2.

F-doped HA ($Ca_{10}(PO_4)_6F_2$) is more resistant to decomposition than the pure HA after the sintering at high temperatures, consistent with the reduced decomposition of HA after the incorporation of some fluoride ions (from MgF_2) for hydroxyl ions.

5. Conclusions

Porosities of sintered HA and PSZ composites were reduced by the addition of 5% MgF_2 to the green powder mixture. PSZ with MgO increased the high temperature decomposition of HA, leading to higher porosity; and the substitution of F^- ions from the MgF_2 for OH^- ions in the HA structure suppressed the decomposition of HA, resulting in lower porosity of the sintered composites, improved micro-hardness and higher phase stability. Substitution of F^- ions for OH^- ions in HA was verified by the shrinkage of the lattice volume of the doped HAs. HA and PSZ composites with MgF_2 had promising results with respect to its densification, hardness and phase stability. More studies should be done about the composites with MgF_2 to investigate their response to bone cells and their biocompatibility. In vitro cell attachment studies of the composites of HAP and PSZ with 5 wt% MgF_2 should be studied. If this gives promising results, these composites can be tested as an implant in vivo under load bearing areas.

Acknowledgements

The authors would like to thank to Mr. A. Sen for X-ray measurements and Mr. A. Nazim for SEM studies at Gebze Institute of Technology.

References

1. Halouani, R., Bernache-Assolant, D., Champion, E. and Ababou, A., Microstructure and related mechanical properties of hot pressed hydroxyapatite ceramics. *J. Mater. Sci.: Mater. Med.*, 1994, **5**, 563–568.
2. Thomas, M. B. and Doremus, R. H., Fracture strength of dense hydroxylapatite. *Am. Ceram. Soc. Bull.*, 1981, **60**, 258–259.
3. Matsuno, T., Watanabe, K., Ono, K. and Koishi, M., Preparation of laminated hydroxyapatite/zirconia sintered composite with the gradient composition. *J. Mater. Sci. Lett.*, 1998, **17**, 1349–1351.
4. Kim, H. W., Noh, Y. J., Koh, Y. H., Kim, H. E. and Kim, H. M., Effect of CaF_2 on densification and properties of hydroxyapatite–zirconia composites for biomedical applications. *Biomaterials*, 2002, **23**, 4113–4121.
5. Li, J., Liao, H. and Hermansson, L., Sintering of partially-stabilized zirconia and partially-stabilized zirconia–hydroxyapatite composites by hot isostatic pressing and pressureless sintering. *Biomaterials*, 1996, **17**, 1787–1790.
6. Heimann, R. B. and Vu, T. A., Effect of CaO on thermal decomposition during sintering of composite hydroxyapatite–zirconia mixtures for monolithic bioceramic implants. *J. Mater. Sci. Lett.*, 1997, **16**, 437–439.
7. Rao, R. R. and Kannan, T. S., Synthesis and sintering of hydroxyapatite–zirconia composites. *Mater. Sci. Eng. C*, 2002, **20**, 187–193.

8. Rapacz-Kmita, A., Slosarczyk, A. and Paszkiewicz, Z., Mechanical properties of HAp–ZrO_2 composites. *J. Eur. Ceram. Soc.*, 2006, **26**, 1481–1488.
9. Nath, S., Sinha, N. and Basu, B., Microstructure, mechanical and tribological properties of microwave sintered calcia-doped zirconia for biomedical applications. *Ceram. Int.*, 2008, **34**, 1509–1520.
10. Rapacz-Kmita, A., Slosarczyk, A., Paszkiewicz, Z. and Paluszkiewicz, C., Phase stability of hydroxyapatite–zirconia (HAP–ZrO_2) composites for bone replacement. *J. Mol. Struct.*, 2004, **704**, 333–340.
11. Zhang, J., Iwasa, M., Kotobuki, N., Tanaka, T., Hiroso, M., Ohgushi, H. *et al.*, Fabrication of hydroxyapatite–zirconia composites for orthopedic applications. *J. Am. Ceram. Soc.*, 2006, **89**, 3348–3355.
12. Kumar, R., Prakash, K. H., Cheang, P. and Khor, K. A., Microstructure and mechanical properties of spark plasma sintered zirconia–hydroxyapatite nano-composite powders. *Acta Mater.*, 2005, **53**, 2327–2335.
13. Chang, E., Chang, W. J., Wang, B. C. and Yang, C. Y., Plasma spraying of zirconia–reinforced hydroxyapatite composite coatings on titanium. *J. Mater. Sci.: Mater. Med.*, 1997, **8**, 193–200.
14. Evis, Z., Sato, M. and Webster, T. J., Increased osteoblast adhesion on nanograined hydroxyapatite and partially stabilized zirconia composites. *J. Biomed. Mater. Res. A*, 2006, **78A**, 500–507.
15. Inuzuka, M., Nakamura, S., Kishi, S., Yoshida, K., Hashimoto, K., Toda, Y. *et al.*, Hydroxyapatite-doped zirconia for preparation of biomedical composites ceramics. *Solid State Ionics*, 2004, **172**, 509–513.
16. Nayak, Y., Rana, R., Pratihar, S. and Bhattacharyya, Low-temperature processing of dense hydroxyapatite–zirconia composites. *Int. J. Appl. Ceram. Technol.*, 2008, **5**, 29–36.
17. Wu, J. M. and Yeh, T. S., Sintering of hydroxyapatite–zirconia composite material. *J. Mater. Sci.*, 1988, **23**, 3771–3777.
18. Khalil, K. A., Kim, S. W. and Kim, H. Y., Consolidation and mechanical properties of nanostructured hydroxyapatite–(ZrO_2+3 mol% Y_2O_3) bioceramics by high-frequency induction heat sintering. *Mater. Sci. Eng. A*, 2007, **456**, 368–372.
19. Takagi, M., Mochida, M., Uchida, N., Saito, K. and Uematsu, K., Filtered cake and hot isostatic pressing for tzp-dispersed hydroxyapatite sintering. *J. Mater. Sci.: Mater. Med.*, 1992, **3**, 199–203.
20. Adolfsson, E., Alberius-Henning, P. and Hermansson, L., Phase analysis and thermal stability of hot isostatically pressed zirconia–hydroxyapatite composites. *J. Am. Ceram. Soc.*, 2000, **83**, 2798–2802.
21. Silva, V. V., Lameiras, F. S. and Domingues, R. Z., Microstructured and mechanical study of zirconia–hydroxyapatite (ZH) composite ceramics for biomedical applications. *Compos. Sci. Technol.*, 2001, **61**, 301–310.
22. Zi, J., Ziao, H. and Hermansson, L. H., Sintering of partially-stabilized zirconia and partially-stabilized zirconia–hydroxyapatite composites by hot isostatic pressing and pressureless sintering. *Biomaterials*, 1996, **17**, 1787–1790.
23. Evis, Z., Ergun, C. and Doremus, R. H., Hydroxylapatite–zirconia composites: thermal stability of phases and sinterability as related to the CaO–ZrO_2 diagram. *J. Mater. Sci.*, 2005, **40**, 1127–1134.
24. Delgado, J. A., Martinez, S., Ginebra, M. P., Morejon, L., Carlsson, N., Fernandez, E. *et al.*, Mechanical behaviour of new zirconia–hydroxyapatite ceramic materials. *Key Eng. Mater.*, 2001, **192–195**, 151–154.
25. Evis, Z., Reactions in hydroxyapatite zirconia composites. *Ceram. Int.*, 2007, **33**, 987–991.
26. Evis, Z., Al^{3+}-doped nano-hydroxyapatites and their sintering characteristics. *J. Ceram. Soc. Jpn.*, 2006, **114**, 1001–1004.
27. Hilliard, J. E., Estimating grain size by the intercept method. *Met. Prog. Data Sheet*, 1964, 99.
28. Cullity, B. D., *Elements of X-ray Diffraction* (*second edition*). Addison-Wesley Publishing Company, Reading, MA, 1978, pp. 411–415.
29. Hubbard, C. R., Evans, E. H. and Smith, D. K., The reference intensity ratio, I/I_c, for computer simulated powder patterns. *J. Appl. Crystallogr.*, 1976, **9**, 169–174.
30. Young, R. A., Implications of atomic substitutions and other structural details in apatites. *J. Dental Res.*, 1974, **53**, 193–203.
31. Evis, Z. and Doremus, R. H., Effect of MgF_2 on hot pressed hydroxyapatite/monoclinic zirconia composites. *J. Mater. Sci.*, 2007, **42**, 3739–3744.
32. Elliott, J. C., *Structure and Chemistry of the Apatites and Other Calcium Orthophosphates*. Elsevier, NY, 1994, p. 161.
33. Narasaraju, T. S. B. and Phebe, D. E., Some physico-chemical aspects of hydroxylapatite. *J. Mater. Sci.*, 1996, **31**, 1–21.
34. Kay, M. I., Young, R. A. and Posner, R. S., Crystal structure of hydroxyapatite. *Nature*, 1964, **204**, 1050–1052.
35. Hughes, J. M. and Rakovan, J., The crystal structure of apatite, $Ca_5(PO_4)_3$(F,OH,Cl). In *Phosphates Geochemical and Materials Importance. Reviews in Mineralogy & Geochemistry*, ed. M. J. Kohn, J. Rakovan and J. M. Hughes, 2002, pp. 1–12.